行政院國家科學委員會專題研究計畫 成果報告

感測網路分散式機器人研發--子計畫一：救援機器人之設計與結構分析(3/3)
研究成果報告(完整版)

計 畫 類 別 ：整合型
計 畫 編 號 ：NSC 98-2218-E-216-001-
執 行 期 間 ：98 年 08 月 01 日至 99 年 07 月 31 日
執 行 單 位 ：中華大學應用統計學系

計 畫 主 持 人：楊立杰

報 告 附 件 ：出席國際會議研究心得報告及發表論文

公 開 資 訊 ：本計畫可公開查詢

中 華 民 國 99 年 10 月 31 日

行政院國家科學委員會補助專題研究計畫 ■成果報告 □期中進度報告

感測網路分散式機器人研發--子計畫一：救援機器人之設計與結構分析(3/3)

計畫類別：□ 個別型計畫　■ 整合型計畫
計畫編號：NSC 98-2218-E-216-001
執行期間： 98 年 8 月 1 日至 99 年 7 月 31 日

計畫主持人：楊立杰
共同主持人：
計畫參與人員：

成果報告類型(依經費核定清單規定繳交)：□精簡報告 ■完整報告

本成果報告包括以下應繳交之附件：
□赴國外出差或研習心得報告一份
■赴大陸地區出差或研習心得報告一份
■出席國際學術會議心得報告及發表之論文各一份
□國際合作研究計畫國外研究報告書一份

處理方式：除產學合作研究計畫、提升產業技術及人才培育研究計畫、列管計畫及下列情形者外，得立即公開查詢
□涉及專利或其他智慧財產權，□一年□二年後可公開查詢

執行單位：中華大學應用數學系

中 華 民 國 99 年 10 月 31 日

行政院國家科學委員會專題研究計畫成果報告

感測網路分散式救援機器人研發—子計畫一：救援機器人之設計與結構分析(3/3)

Design and Structure Analysis of Rescue Robot

計畫編號：NSC 98-228-E-216-001

執行期限：98 年8 月1 日至99 年7 月31 日

主持人：楊立杰中華大學應用數學所

E-mail: young@chu.edu.tw

一、中文摘要

本計畫用三年的時間，利用邊界元素法，針對救援型機器人做了有效的減重分析。首先分析在機器人的設計上具有許多不同大小的環形工件，在承受反向壓力後所產生塑性鉸的位置，塑性鉸的個數將會隨著受力的增加，以及不同的裂縫位置，而在圓環的不同位置產生，事實上，當圓環塑性鉸增加到四個時，此圓環便會崩塌。另外，也針對救難機器人的支撐架做應力分析。在救援機器人的救援過程中，機器人本身的輕巧性對救援過程的成敗佔有非常重要的影響力，也因此，本計畫的第二個階段便是應用邊界元素法，針對目前所設計的救援機器人中較大的元件加以裁剪，並做應力分析，進而達到減重的效果，側面的懸吊板正是本計畫要分析的元件，結果證明經過裁剪後的機器人重量只有原來的三分之二，但強度仍在安全範圍之內，因而達到減重的效果。減重是可以適用在救援型機器人的任何一個工件的，第三個階段便是應用邊界元素程式分析，將救援機器人所使用的齒輪的材料，由鋁合金(楊式係數 72GPa，密度 2.7 g/cm^3)改為塑鋼(楊式係數 2.5GPa，密度 1.42 g/cm^3)，而達到救援機器人的重量再向下修改的目的。

關鍵詞：邊界元素法

Abstract

Boundary Element Method (BEM) is employed in this project for three years to get a significant result about weight reduction of the rescue robot. First of all we focus on the circular ring which is the most popular specimen in the rescue robot to demonstrate that the location of a crack can strongly affect the sequence of plastic hinge development which in turn affects crack stability of a structure. A specific example of an elastic-plastic ring loaded with diametrically opposite concentrated loads is employed to investigate these effects. In fact, the ring will collapse if the number of plastic hinges is up to four. In addition, the stress analysis in the supporting frame of the rescue robot is also finished. The next step is the weight reduction of the largest portion of the rescue robot, i.e., the lateral plate without causing the strength of it by using the Boundary Element Method. The dynamical loading conditions are performed before and after weight reduction. The numerical results of the stress distribution and the plastic deformation along the center line (interface) of the lateral plate show that the weight of the plate is reduced to two thirds of the original and the endure limits of the plate before and after weight reduction are almost the same and therefore, will not lower the strength of the plate. The final step of the project is to replace the material of the

gears of the rescue robot from Aluminum Alloy (Young's modulus 72GPa, density2.7 g/cm^3) by Polyacetal (POM) (Young's modulus 2.5 GPa, density 1.42 g/cm^3) and therefore, reduce the weight of the rescue robot to three quarters of the original weight.

Keyword: Boundary Element Method, Polyacetal (POM).

二、Background

The first step in the BEM solution is to divide the specimen into two bodies, referred to below as the interface. The interaction between the two bodies is included through boundary conditions relating the displacements and stresses on either side of the interface, i.e., the 2 displacement components and the 2 stress components must be continuous. Thus, at each pair of points on the interface we have four conditions involving eight quantities. Four of those are eliminated algebraically using the boundary condition, thus leaving four unknowns at each pair. Two coupled boundary integral equations, written as a function of position on the boundary of a body, enforce all of the field equations of elasticity for that body. The two equations for each of the two artificially divided bodies are applied to each discrtized point on the interface, thus giving four equations and four unknowns at each pair of interface points. If the boundary of either of the artificially divided bodies consists of other than common interface, then at each of these boundary points there are four boundary quantities to be accounted for. The only condition we have used on these external boundaries has been prescribed stress, thus leaving the two displacements as unknowns, with two equations provided by that body's two boundary integral equations. The BEM consists of the discretization of the boundary surfaces and the numerical approximation of the boundary quantities in the set of equations obtained from boundary integrals as described above. We model the boundary, using straight-line elements, centered about nodes at which the integral equations are applied in [1]. For straight boundary this introduces no approximations. We assume that the stress and displacement are constants resulting in integrals of the known 2D Green's function which have been evaluated in closed form in [1]. The final result is a system of simultaneous linear algebraic equations for the unknowns nodal displacements and stresses.

It is known theoretically in [2] that the elastic-plastic analysis of statically indeterminate structures of long slender members in bending, from first yield to limit load, involves a sequential formation of plastic hinges at intermediate loads. The total member of plastic hinges becomes the degree of statical indeterminacy plus one at collapse. The objectives of this research to demonstrate that the location of the crack can strongly affect the sequence of plastic hinge development numerically, as well as the crack location, affects crack stability. With these objectives in mind, the analysis shall proceed to establishing the BEM codes for development of the first, second, and third plastic hinges, respectively.

Earthquakes are so frequently in the world recently which always causing serious damage of the buildings, properties, and injury and death of peoples. Rescue robots with light, thin body are therefore needed in small space of the disaster scene. During weight reduction process the strength of the rescue robot is also evaluated. Several papers show the potential applications of the BEM code to crack problems. Ghorbanpoor and Zhang [1] point out that the accuracy of the BEM prediction is satisfactory when it is compared with results from a finite element solution with very fine mesh and with the analytical solution. Tan and Gao [2] show the powerful application of the BEM in the analysis of biomaterial interface crack problem. Lih-jier Young [3] show the powerful application of the BEM in rough contact mixed mode with the plastic crack tip problem and gives the accuracy up to 98.11%. Boundary element method is used to model the complex resistance to the applied field of the lateral plate of rescue robot to find the stress distribution along the interface. The outlook and dimension in mm of the plate are shown in Fig. 1. Paper in [4] also shows the potential application of the BEM determining the effect of crack face roughness in a realistic experimental specimen. The maximum allowable stress of the plate is defined by both the normal and the shear stress of first point along the interface reach the yield stress σ_y and τ_y, respectively, where $\tau_y = \sigma_y/\sqrt{3}$. The plastic displacement of the interface is obtained by increasing the loading of the plate after the first point yield. Keep increasing the loading and we can get the plastic displacement of the interface.

In fact, the physical and mechanical properties of Polyacetal (POM) are quiet excellent. Due to these properties, i.e., low wear rate and small friction coefficient (0.1 ~ 0.3) POM can be effectively applied in the gear (Figure 10) and bearings in the occasion to be a high degree of wear. POM with high rigidity, high strength, and fatigue resistance has similar properties as of the soft metal which can be applied occasionally to replace the soft metal.

三、Results

The ring and its loading are doubly symmetric and the crack is located by from the horizontal as in Fig. 1. The mean radius of the ring is R and its radial thickness is t, and it is assumed to be of uniform unit thickness perpendicular to its plane. P is the load and locates any section around the ring from the horizontal. It is assumed that the ring is long and slender, $R/t \geq 10$, so that deformation due to in-plane bending is the only significant deformation. The present model is discretized into 260 points and 4 regions (I_1-I_4) of different types of boundary conditions for the cracked ring shown in Fig. 2. As mentioned in [1], the cracked body is divided into two parts by $B\gamma$ ($\gamma = 1,2$) denote the boundary traction and displacement components, respectively; and I_1 the crack region and I_2 the ligament region of the interface. The boundary condition of I_2 must satisfy the continuity of the stresses and displacements on either side of the interface, i.e., $({}_2t_1)_{I2} = -({}_1t_1)_{I2}$, and $({}_2t_2)_{I2} = -({}_1t_2)_{I2}$, $({}_2u_1)_{I2} = -({}_1u_1)_{I2}$, and $({}_2u_2)_{I2} = -({}_1u_2)_{I2}$. The unknowns are $({}_1t_1)_{I2}$, $({}_1t_2)_{I2}$, $({}_1u_1)_{I2}$ and $({}_1u_2)_{I2}$. The boundary conditions for open crack $I1$ and the free surface I_4 are zero stress, i.e., $({}_\gamma t_1)_{I1,I4} = -({}_\gamma t_2)_{I1,I4} = 0$ and the unknowns are $({}_\gamma u_1)_{I1,I4}$ and $({}_\gamma u_2)_{I1,I4}$, where $\gamma = 1,2$ depending on whether that portion is B_1 or B_2. The unknowns boundary components can be obtained by using the Gaussian elimination method after converting boundary conditions into the final matrix form. As a first approximation of the moments in a cracked elastic ring, the internal moments, M_0, in an "uncracked" ring is used. Table 1 shows the comparison of the theoretical results for M_0/PR in the uncracked ring with the numerical one (BEM model). It is quiet clear that the numerical accuracy M_0/PR goes from 91.18% at $\theta = 60°$ to 99.13% at $\theta = 30°$. It is noted that according to [2] for $a/t = 0.3$, the relaxation of moments caused by the crack's elastic stiffness reduction is 4% or less, but for deeper cracks such as $a/t = 0.5$, the relaxation is as much as 30%. We can get the same result by inspecting Table 2 and comparing it with Table 1 for the BEM values.

(一) Development of the first plastic hinge

As mentioned in [2], if we want to find the load, P_1, at which the first hinge forms and its location, it is denoted that the ring can be analyzed as completely elastic up to that load. As a first approximation of the moments in a cracked elastic ring, the internal moments, M_0, in an "uncracked" ring is used. The elastic solution for the uncracked ring gives the results for M_0/PR in Table 1. However, the crack reduced the stiffness of the ring at the cracked section, causing a redistribution of the moment in the ring and is analyzed by the superposition in [2] and the BEM methods. In finding the first hinge location it is worthy to be mention that we have to add one more boundary between the outer and the inner boundaries of the ring as shown in Fig. 3. Therefore, we can compute the resulting moment at each nodal point of the new boundary and then get the location of the maximum moment (first hinge). The model is discretized into 256 points and 4 regions (I_1- I_5) of different types of boundary conditions. As described above I_1 is the crack region and I_2, I_5 are the ligament regions of the interface. The boundary condition of I_2 and I_5 must satisfy the continuity of the stresses and displacements on either side of the interface, i.e., $({}_2t_1)_{I2,I5}=-({}_1t_1)_{I2,I5}$ and $({}_2t_2)_{I2,I5}=-({}_1t_2)_{I2,I5}$, $({}_2u_1)_{I2,I5}=-({}_1u_1)_{I2,I5}$, and $({}_2u_2)_{I2,I5}=-({}_1u_2)_{I2,I5}$. The unknowns are $({}_1t_1)_{I2,I5}$, $({}_1t_2)_{I2,I5}$, $({}_1u_1)_{I2,I5}$ and $({}_1u_2)_{I2,I5}$. The boundary conditions for open crack I_1 and the free surface I_4 are zero stress, i.e., $({}_\gamma t_1)_{I1,I4}=-({}_\gamma t_2)_{I1,I4}=0$ and the unknowns are $({}_\gamma u_1)_{I1,I4}$ and $({}_\gamma u_2)_{I1,I4}$, where $\gamma=1,2$ depending on whether that portion is B_1 or B_2. The unknowns boundary components can also be obtained by using the Gaussian elimination method.

Table 2 shows the comparison between the theoretical and the BEM values of M/PR for different *a/t* and $\alpha=0°$. It has been seen that the accuracy is in the range of 93.24% to 99.99%. It has been assumed in [2] that the crack is into the inside or outside of the ring, so that it is on the tension side for each location. Also notice that the first hinge occurs at the crack location, when that location is at a relatively high moment in the uncracked ring, that is $\theta=0°$ to 15°and $\theta=75°$ to 90°. However, for locations with relatively low moment, the first hinge forms at the maximum moment location, $\theta=90°$. Finally, it is noted that the first hinge load P_1, is affected appreciably only when the first hinge forms at the crack location. Upon comparing the values of M/PR in Table 2 with Table 1, the effects of changes of elastic moment stiffness of the "cracked element" are also noted to be appreciable only when the crack is placed at a relatively high moment position. Of course, this effect would increase with larger *a/t* values (*a/t*=0.3 in Table 2), but for this example it is really quite small.

(二)Development of the second plastic hinge

In an uncracked ring, the second hinge development at the same time as the first hinge, at the load points or points of maximum moment. Again the elastic superposition in [2] and the BEM methods can be used even though a first hinge is already formed. The boundary conditions of the hinge point are just set the values of the two stress components which leave the two displacements unknown. Table 3 has been prepared theoretically and numerically. The accuracy is in the range of 70.06% to 99.99%.

(三) Development of the third plastic hinge

Once again, the formation of the full analysis at the instant of development of the third plastic hinge can be done using the 2D BEM method as above. For the border perspective, it is more relevant to combine Table 2-4 into a composite of the sequence of hinge formation as affected by the crack location. This is given as Table 5. The notations, 1 through 4, indicate the first through fourth hinges formed, respectively. The notations, 2, 3, and 3, 4 indicate simultaneous formation of two hinges, symmetric case of no crack. Indeed, the widely varied pattern of the sequence of hinge formation in Table 5 is quite surprising. Simply, the change of the crack location (for a given crack size, *a/t*=0.3, and ring slenderness ratio, *R/t*=10) causes this wide variation in the pattern. Moreover, expect for having the crack at the load point, $\alpha=90°$, the relative loads for hinge formation do not vary greatly (less than 10% except for the first hinge for $\alpha=75°$□, near the load point). This seems quite surprising in view of the wide variety of hinge sequences.

(四)Development of the fourth plastic hinge

Theoretically as in [2], the fourth (last) hinge forms either 180°□or 0°□, which means that an elastic path connects the load points up until the fourth hinge forms. Since this method computes the elastic bending moments on that elastic path, the relative load point displacements can easily be computed for each successive hinge formation load, including the fourth hinge. Thus, a complete load-displacement diagram may be constructed, since that diagram is linear between successive hinge formation loads. Figure 5 shows the supporting frame of the rescue robot which is discretized into 222 nodal points and 6 regions (I_1- I_7) of different types of boundary conditions. As mentioned before, The boundary conditions of I_2 are $({}_2t_1)_{I2}=-({}_1t_1)_{I2}$, and $({}_2t_2)_{I2}=-({}_1t_2)_{I2}$, $({}_2u_1)_{I2}=-({}_1u_1)_{I2}$, and $({}_2u_2)_{I2}=-({}_1u_2)_{I2}$ and the unknowns are $({}_1t_1)_{I2}$, $({}_1t_2)_{I2}$, $({}_1u_1)_{I2}$ and $({}_1u_2)_{I2}$. The upper and right pins are assumed fixed. A compressive load is applied through the lower pin in the positive x_1 direction by assuming a uniform distribution of normal traction over 90° of lower pin hole surface, i.e., points 214, 215, 216, 217, and 218 (I_4). Therefore, the boundary conditions of these points are $({}_2t_1)_{I2}=p\cos\theta_1$ and $({}_2t_2)_{I2}=p\sin\theta_1$. The unknowns are $({}_2u_1)_{I4}$ and $({}_2u_2)_{I4}$, where p is applied normal stress on the lower hole and θ_1 is the angle between the direction normal of each node and x_1-axis. The boundary conditions of the free surface I_5 are $({}_\gamma t_1)_{I5}=-({}_\gamma t_2)_{I5}=0$, and the unknowns are $({}_\gamma u_1)_{I5}$ and $({}_\gamma u_2)_{I5}$. In order to have zero shear stress on the hole, the horizontal displacement component of points 110, 111, 98, 99, 220, 137, 138, 139 and 140 ($I6$) is taken to be zero and their two traction components are related by $\tan\theta_2$, where θ_2 is the angle between the direction normal and x_1-axis, in order to have zero shear stress on the hole. Hence the boundary conditions for points on $I6$ in the upper half plane are $({}_1u_1)_{I6}=0$, $({}_1t_2)_{I6}=({}_1t_1)_{I6}, \tan\theta_2$ and the unknowns are $({}_2u_2)_{I6}$, $({}_2t_1)_{I6}$. Point 97 (I_7) is totally fixed point. The boundary conditions of this point are $({}_1u_1)_{I7}=({}_1u_2)_{I7}=0$ and the unknowns are $({}_1t_7)_{I7}$, $({}_1t_2)_{I7}$. This combination of boundary conditions results in a free body diagram of the form given in Figure 5(b). The unknowns boundary components can be obtained by using the Gaussian elimination method. Figure 6 shows the displaced position of the interface of the specimen. The majority of the displacement shown is normal to the interface and the motion parallel to the interface cannot be seen on the scale shown in this figure. It can be seen, and expected from Figure 5(b), that the ligament portion of the interface is rotated about 0.01° counterclockwise from horizontal.

(五) Dynamical Loading Conditions before Weight Reduction of Lateral Plate

As discussed in [5], the first step in the BEM solution is to divided the homogeneous medium into two bodies B_γ ($\gamma=1,2$) along the center line which we call the interface as shown in Fig. 8(a). The interaction between the two bodies included through boundary conditions relating the displacements and stresses on either side of the interface. Let ${}_\gamma t_i$ and ${}_\gamma u_i$ ($\gamma=1,2$ and $i=1,2$) denote the ith boundary traction and displacement components, respectively, on the boundary of B_γ. The present model is discretized into 648 nodal points and 4 regions (I_2, I_4, I_5, and I_6) of different types of boundary conditions shown in Fig. 8(a). The interface is denoted by I_2. At points on this region the 2 displacement components and 2 stress components must be continuous. Therefore, the boundary conditions are $({}_2t_1)_{I_2}=-({}_1t_1)_{I_2}$ and $({}_2t_2)_{I_2}=-({}_1t_2)_{I_2}$, $({}_2u_1)_{I_2}=({}_1u_1)_{I_2}$ and $({}_2u_2)_{I_2}=({}_1u_2)_{I_2}$. This leaves $({}_1t_1)_{I_2}$, $({}_1t_2)_{I_2}$, $({}_1u_1)_{I_2}$ and $({}_1u_2)_{I_2}$, as the unknowns. Compressive loads are applied through the six pins as in Fig. 9(a) by assuming a uniform distribution of normal traction over 90° of pin hole surfaces (I_6). Therefore, the boundary conditions of these points are $({}_\gamma t_1)_{I_6}=p\cos\theta$ and $({}_\gamma t_2)_{I_6}=p\sin\theta$. The unknowns are $({}_\gamma u_1)_{I_6}$ and $({}_\gamma u_2)_{I_6}$, where p is applied normal stress on the six holes and θ is the angle between the direction normal of each node and x_1-axis as in Fig.

8(a). A concentrate load is also applied through lower half plane point 110 (I_4) The boundary conditions are $({}_1t_2)_{I_4} = p$, $({}_2t_1)_{I_4} = ({}_2t_2)_{I_4} = ({}_1t_1)_{I_4} = 0$ and the unknowns are $({}_\gamma u_1)_{I_4}$ and $({}_\gamma u_2)_{I_4}$. The boundary conditions of the free surfaces (I_5) are $({}_\gamma t_1)_{I_5} = ({}_\gamma t_2)_{I_5} = 0$, and the unknowns are $({}_\gamma u_1)_{I_5}$ and $({}_\gamma u_2)_{I_5}$, where $\gamma = 1$ or 2 depending on whether that portion of I_5 is in B_1 or B_2. Once the points on the interface yield (I_8) in shear direction the boundary conditions are $({}_1t_1)_{I_8} = \sigma_y/\sqrt{3}$, $({}_2t_1)_{I_8} = -\sigma_y/\sqrt{3}$, $({}_1t_2)_{I_8} = -({}_2t_2)_{I_8}$ and $({}_1u_2)_{I_8} = ({}_2u_2)_{I_8}$. The unknowns are $({}_2t_2)_{I_8}$, $({}_1u_1)_{I_8}$, $({}_1u_2)_{I_8}$ and $({}_2u_1)_{I_8}$. For the case both the normal and shear directs yield the boundary conditions are $({}_1t_1)_{I_8} = \sigma_y/\sqrt{3}$, $({}_2t_1)_{I_8} = -\sigma_y/\sqrt{3}$, $({}_1t_2)_{I_8} = \sigma_y$ and $({}_2t_2)_{I_8} = -\sigma_y$.

The BEM consists of the discretization of the boundary surfaces and the numerical approximation of the boundary quantities in the set of equation obtained from the boundary integrals. We model the boundary, using straight-line elements, centered about nodes at which the integrals of the 2D Green's function as in [6]. The final system of simultaneous linear algebraic equations for the unknown nodal displacements and stresses, can be obtained by using Gaussian elimination method.

Figure 10(a) shows the shear stress distribution along the interface. It can be seen that the shear stress of point 100 reaches the yielding criteria in (300 MPa) with the applied load $p = -5.4$ MPa. However, the normal stress as shown in Fig. 11(a) is not yield yet. We can keep increasing the applied load to $p = -7.1$ Mpa until the normal stress of point 100 reaches the yielding criteria (520 MPa) as in Fig. 12(a). There are three points, i.e., 100, 99, and 98 yield in shear direction at this moment as shown in Fig. 13(a). Both the shear and normal stresses reach the yielding criteria of points 100, 99, 98, and 97 as in Figs 14(a) and 15(a), respectively, when applied load is up to -7.3 MPa. Figures 16(a) and 17(a) show the plastic displacements both in shear and normal direction of the four yielding point mention above.

(六) Dynamical Loading Conditions after Weight Reduction of Lateral Plate

The model for the weight reduction lateral plate model is discretized into 904 nodal points and 4 regions (I_2, I_4, I_5, and I_6) of different types of boundary conditions shown in Fig. 8(b). All boundary conditions remain the same as described above. In addition, two rectangular regions with the size $80 \times 46\,\text{mm}^2$ have been cut as shown in Fig. 8(b) which reduce the mass of the plate from 3 kg to 2 kg. The boundary conditions of the inner free surface are the same as the outer one (I_5). The final system of simultaneous linear algebraic equations can also be obtained by using Gaussian elimination method.

Figures 10(b) and 11(b) show the stress distribution along the interface. It can be seen from 10(b) that the shear stress of point 228 reaches the yielding criteria in (300 MPa) with the applied load $p = -4.4$ MPa. However, the normal stress as shown in Fig. 11(b) is not yield yet. We can keep increasing the applied load to $p = -5.7$ Mpa until the normal stress of point 111 reaches the yielding criteria (520 MPa) as in Fig. 12 (b). There are three points, i.e., 111, 112, and 228 yield in shear direction at this moment as shown in Fig. 13(b). Both the shear and normal stresses reach the yielding criteria of points 111, 112, and 228, as in Figs 14(b) and 15(b), respectively, when applied load is up to -6.0 MPa. Figures 16(b) and 17(b) show the plastic displacement both in shear and normal direction of the four yielding point mention above.

(七) Stress Analysis of POM Gear with a Crack

There are mainly six different kinds of gear in the rescue robot, i.e., 15T, 22T, 40T, 46T, 65T and 723 mm 0T. The results shown here is the 46T with pitch circle radius, 24 mm addendum circle radius, 11mm root radius and 20° pressure angle as shown in Fig. 18. The present model is discretized into 600 nodal points and 4 regions (I_1, I_2, I_3, and I_5) of different types of boundary conditions shown in Fig. 19. The interface is denoted by I_2. At points on this region the 2 displacement components and 2 stress components must be continuous. Therefore, the boundary conditions are $({}_2t_1)_{I_2} = -({}_1t_1)_{I_2}$ and $({}_2t_2)_{I_2} = -({}_1t_2)_{I_2}$, $({}_2u_1)_{I_2} = ({}_1u_1)_{I_2}$ and $({}_2u_2)_{I_2} = ({}_1u_2)_{I_2}$. This leaves $({}_1t_1)_{I_2}$, $({}_1t_2)_{I_2}$, $({}_1u_1)_{I_2}$ and $({}_1u_2)_{I_2}$, as the unknowns. Compressive load p is action in the direction of line of action shown in Fig. 18. Therefore, the boundary conditions of these points are $({}_1t_1)_{I_3} = p\cos\theta$ and $({}_1t_2)_{I_3} = p\sin\theta$, where θ is the pressure angle of the gear. The unknowns are $({}_1u_1)_{I_3}$ and $({}_1u_2)_{I_3}$. The boundary conditions for open crack I_1 and the free surface I_5 are zero stress, i.e., $({}_\gamma t_1)_{I1,I5} = -({}_\gamma t_2)_{I1,I5} = 0$ and the unknowns are $({}_\gamma u_1)_{I1,I5}$ and $({}_\gamma u_2)_{I1,I5}$, where $\gamma = 1$ for I_1 and $\gamma = 1,2$ for I_5 depending on whether that portion is B_1 or B_2. The unknowns boundary components can also be obtained by using the Gaussian elimination method.

Both Figs 20 and 21 show the opening and shear displacements of the crack of the gear with different materials, respectively. It is obviously that the POM displacement of the crack is much larger than the Aluminum Alloy. Stress singularity at the crack tip is clear shown on Figs 22 and 23 for normal and shear stresses, respectively nevertheless the materials are different. The mode I and mode II stress intensity factors can be calculated according to the formula

$$K_{I,II} = \frac{2u(x_t)G}{\kappa+1}\sqrt{\frac{2\pi}{x_t}} \qquad (1)$$

where $u(x_t)$ is the displacement of the crack tip element, G is the shear modulus, x_t is the coordinate of the crack tip element.The value of κ is $4(1-\nu)$ .for plane strain and $\frac{4}{1+\nu}$ for plane stress, ν is the Poisson Ratio. The results shown on Figs 24 and 25 show both the values of K_I and K_{II} are much larger for POM gear than Aluminum Alloy gear even the weight of POM gear is much lighter.

四、Conclusions

The sequence of plastic hinge formation of a cracked circular ring is investigated by using 2-D boundary element method as the numerical portion to support the theoretical one in [2]. In addition, the stress analysis of the supporting frame of the rescue robot is also finished. It can be seen from the results mentioned above that the weight of one lateral plate of the robot have be reduced 1 kg of mass (from 3 kg to 2 kg) but won't lower the strength that much. (allowable stress is reduced from -7.1 MPa to -5.7 MPa). The total mass of one rescue robot may be reduced at least 2 kg after weight reduction and therefore, can moves nimbly during the rescue process. The specimen made of POM is much lighter than Aluminum Alloy and of course will provide a lighter robot. However, the strength of the specimen may be lowered and therefore, some portion of the specimen with heavy loadings will damage very easily. In fact, how to replace the heavy loading portion of POM specimen by Aluminum Alloy is the next topic of this research.

五、References

[1] Young, L.J. and Tsai, Y.P., 1999. A boundary element application for mixed mode loading idealized sawtooth fracture surface, Int'l J. of Solids and Structures, 36, pp. 3239-3252.

[2] Young, L.J. Plastic hinge development and crack stability analysis in a circular ring, Int'l J. of Solid and Structure, 38, pp. 1355-1367

[3] A. Ghobanpoor and J. Zang, Boundary Elemant Analysis of Crack Growth for Mixed Mode Center Slant Crack Problems, Engineering Fracture

Mechanics, Vol. 36, No.5 pp. 661-668, 1990.

[4] C.L. Tan and Y.L. Gao, Treatment of Bimaterial Interface Crack Problems Using The Boundary Element Method, Engineering Fracture Mechanics, Vol. 36, No. 6, pp. 919-932, 1990.

[5] L.J. Young and Y.P. Tsai, A Boundary Element Application for Mixed Mode Loading Idealized Sawtooth Fracture Surface, Int'l J. of Solids and Structure, 36, 3239-3252, 1999.

[6] L.J. Young, An Analysis of a Fracture Specimen for Rough Crack in Shear, Int'l J. of Fracture, 115, 3, 273~285, 2002.

[7] C.A. Brebbia , J.C.F Telles and L.C. Wrobel, Boundary Element Techniqes , Springer - Verlag,New York,1970.

Figures and Tables

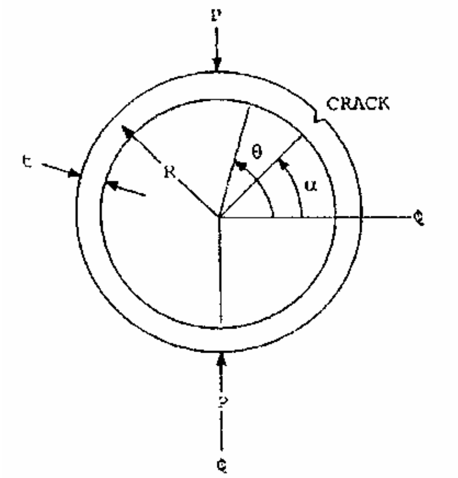

Fig. 1 Cracked ring with diametrically opposite concentrated loads.

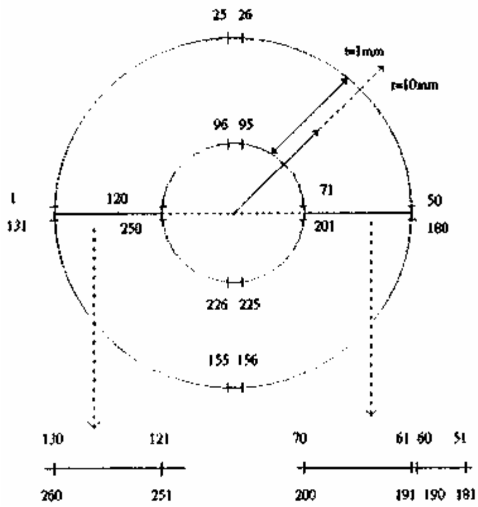

(a)

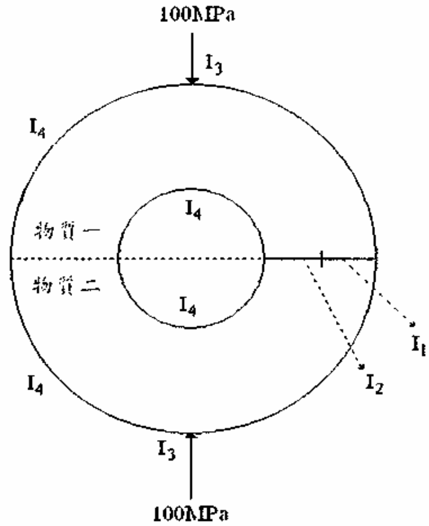

(b)

Fig. 2 Schematic of (a) BEM mesh, (b) different regions of cracked ring.

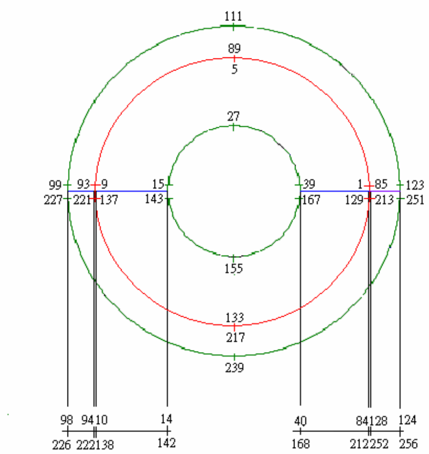

(a)

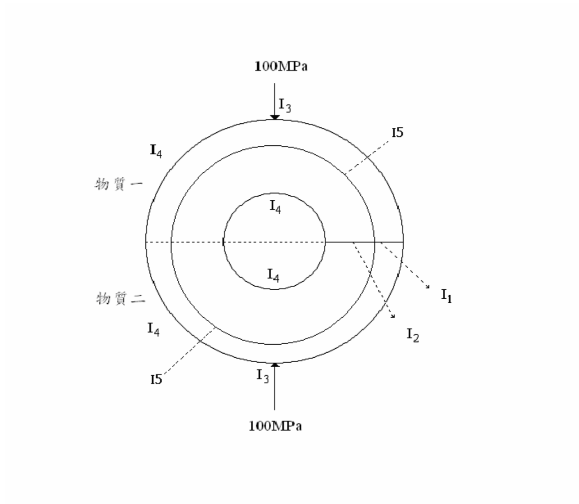

(b)

Fig. 3 Schematic of (a) BEM mesh, (b) different regions of cracked ring with hinges.

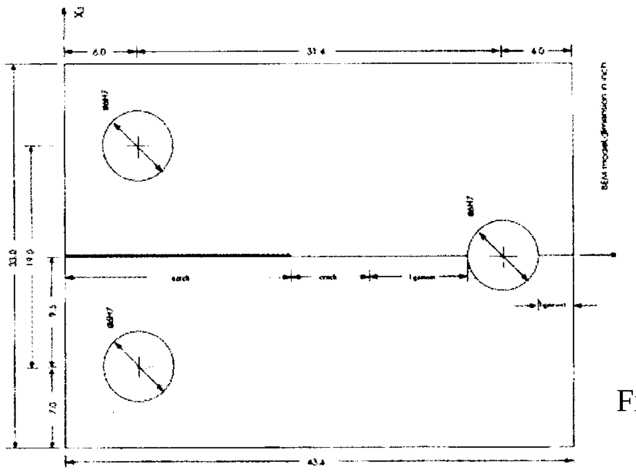

Fig. 4 Supporting frame of rescue robot.

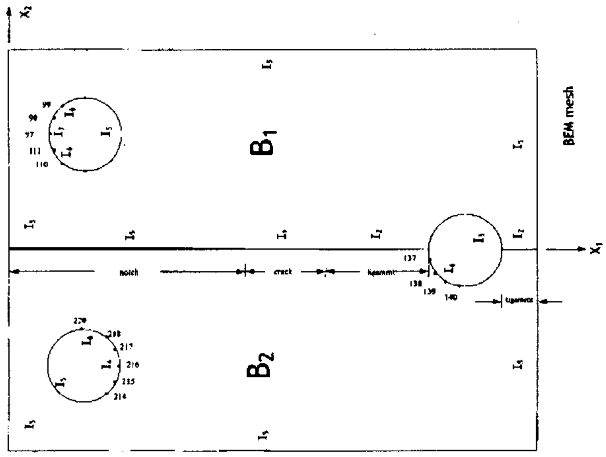

(a)

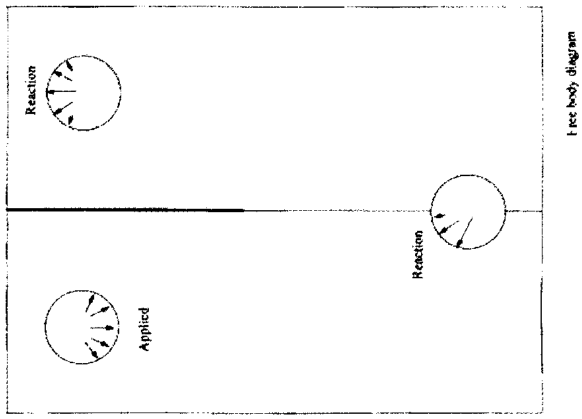

(b)

Fig. 5 Schematic of (a) BEM mesh, (b) free body diagram of supporting frame.

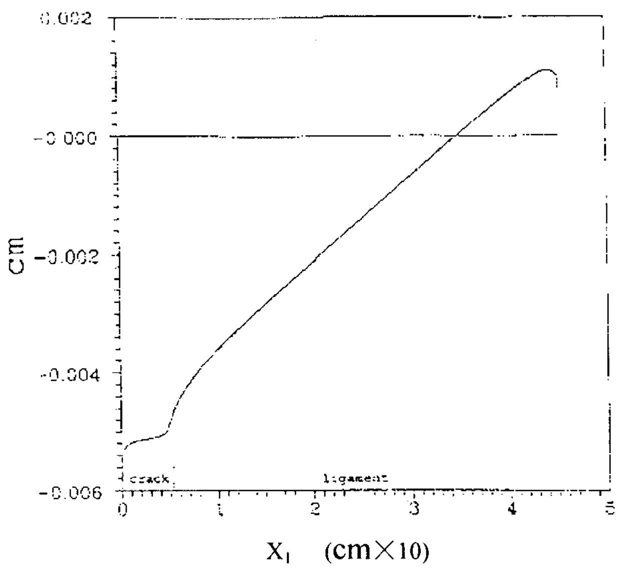

Fig. 6 Displace position of interface of supporting frame.

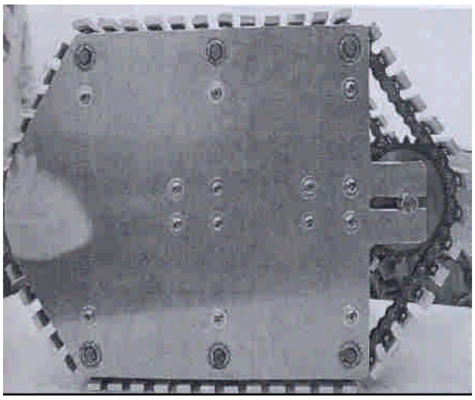

(a)

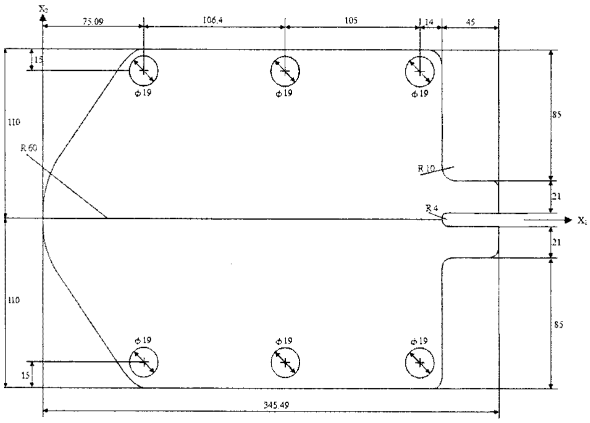

(b)

Fig. 7 (a) Outlook (b) dimension in mm of the lateral plate of rescue robot.

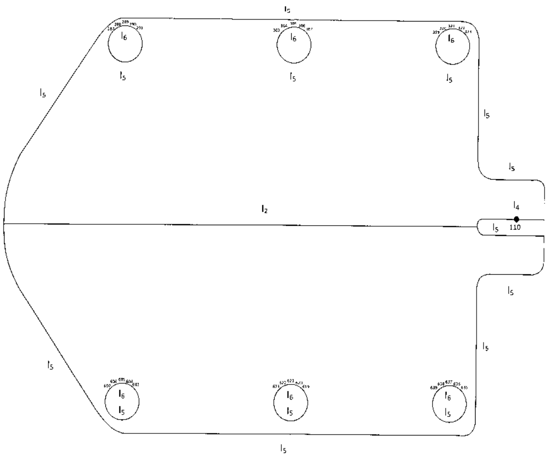

(a)

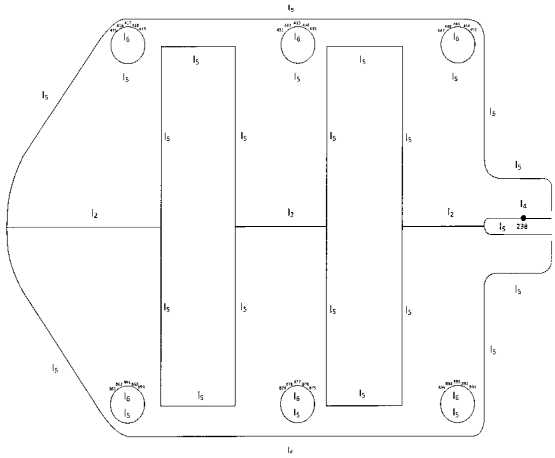

(b)

Fig 8 Schematic of BEM mesh of the lateral plate of rescue robot (a) before (b) after weight reduction.

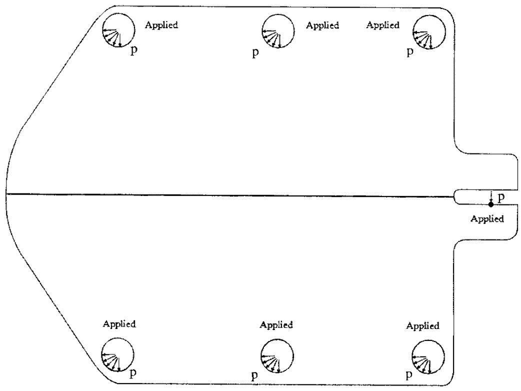

(a)

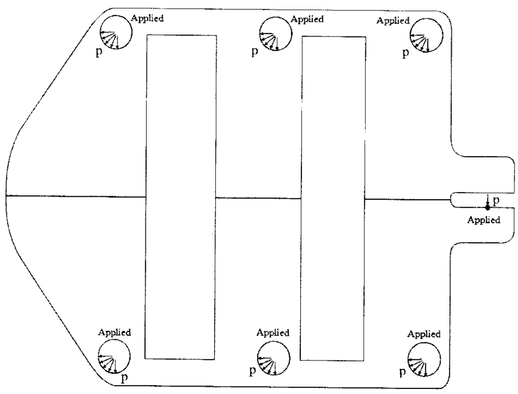

(b)

Fig. 9 Loading conditions of the lateral plate of rescue robot (a) before (b) after weight reduction.

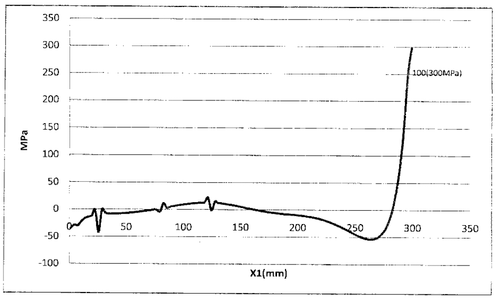

(a)

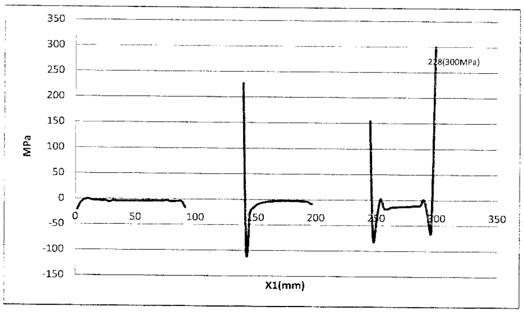

(b)

Fig. 10 Shear stress distribution of the interface of the lateral plate (a) before weight reduction with $p = -5.4$ MPa (b) after weight reduction with $p = -4.4$ MPa.

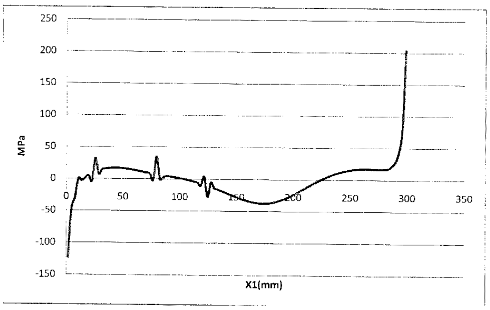

(a)

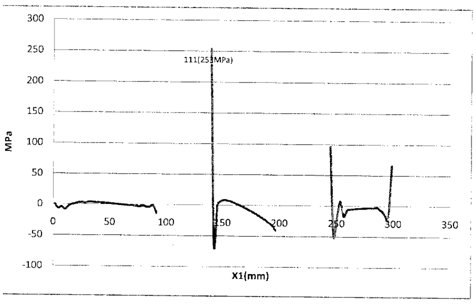

(b)

Fig. 11 Normal stress distribution of the interface of the lateral plate (a) before weight reduction with $p = -5.4$ MPa (b) after weight reduction with $p = -4.4$ MPa.

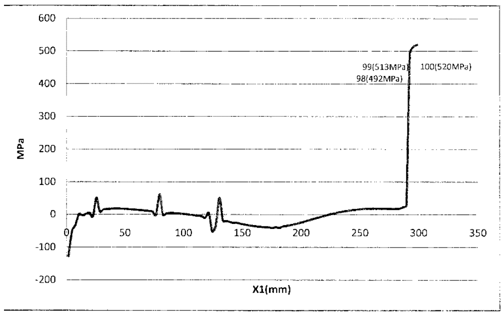

(a)

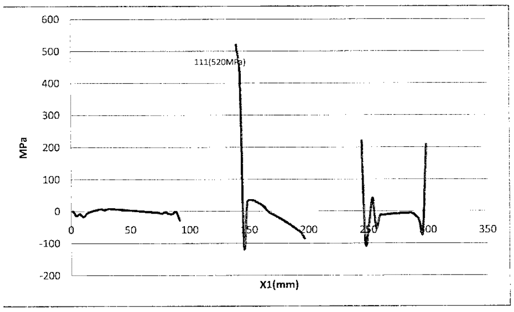

(b)

Fig. 12 Normal stress distribution of the interface of the lateral plate (a) before weight reduction with $p = -7.1$ MPa (b) after weight reduction with $p = -5.7$ MPa.

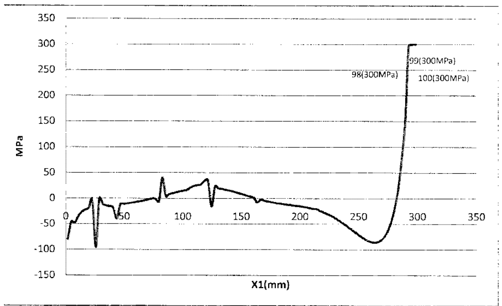

(a)

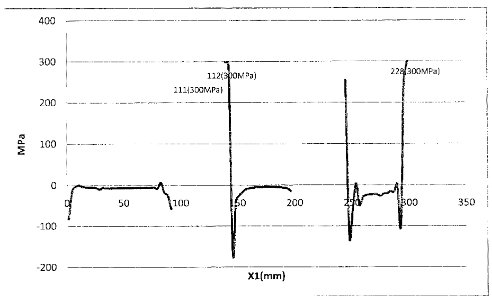

(b)

Fig. 13 Shear stress distribution of the interface of the lateral plate (a) before weight reduction with $p = -7.1$ MPa (b) after weight reduction with $p = -5.7$ MPa

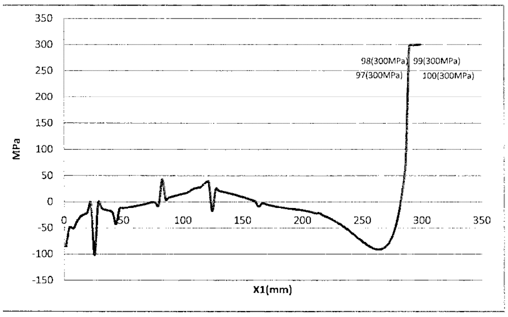

(a)

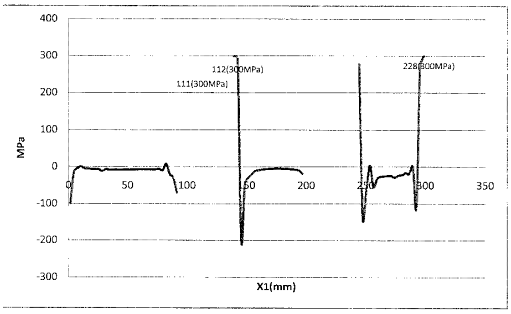

(b)

Fig. 14 Shear stress distribution of the interface of the lateral plate (a) before weight reduction with $p = -7.3$ MPa (b) after weight reduction with $p = -6.0$ MPa.

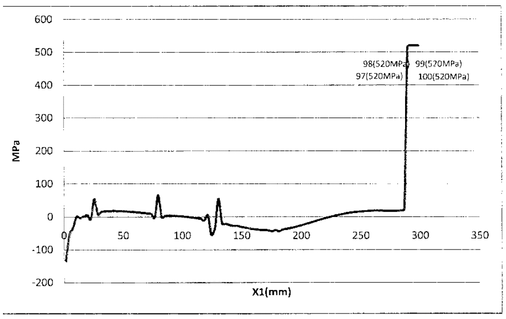

(a)

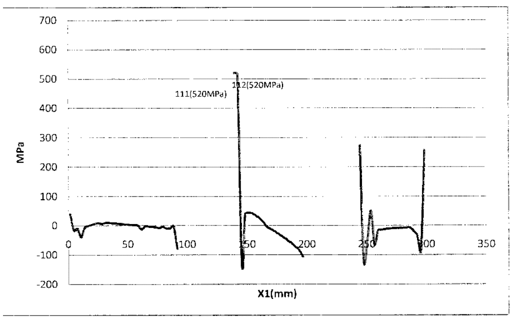

(b)

Fig. 15 Normal stress distribution of the interface of the lateral plate (a) before weight reduction with $p = -7.3$ MPa (b) after weight reduction with $p = -6.0$ MPa.

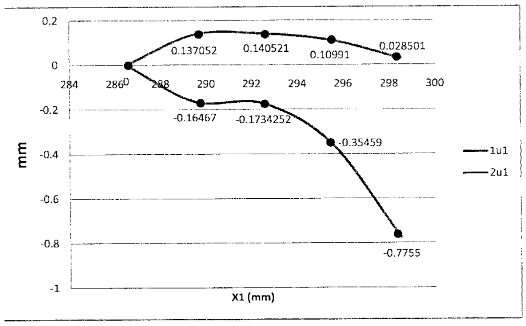

(a)

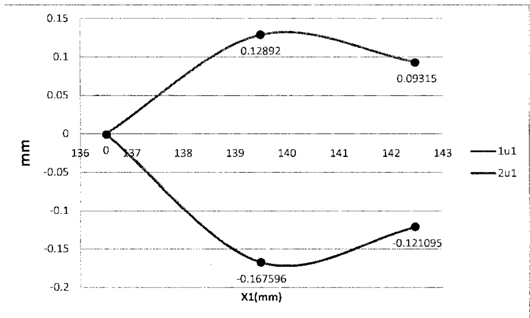

(b)

Fig. 16 Plastic deformation in shear direction of the lateral plate (a) before weight reduction with $p = -7.3$ MPa (b) after weight reduction with $p = -6.0$ MPa.

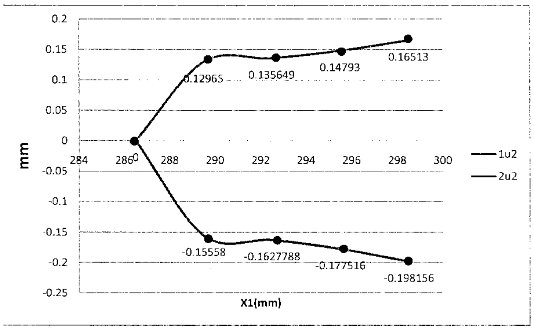

(a)

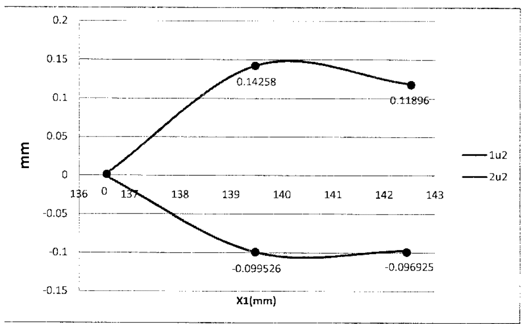

(b)

Fig. 17 Plastic deformation in normal direction of the lateral plate (a) before weight reduction with $p = -7.3$ MPa (b) after weight reduction with $p = -6.0$ MPa.

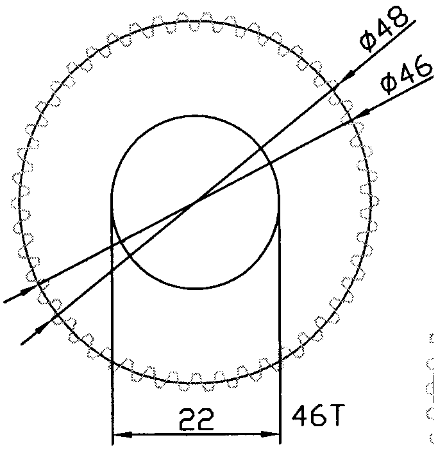

Fig. 18 46T spur g pitch circle radius, 24 mm addendum circle radius, and 20° pressure angle.

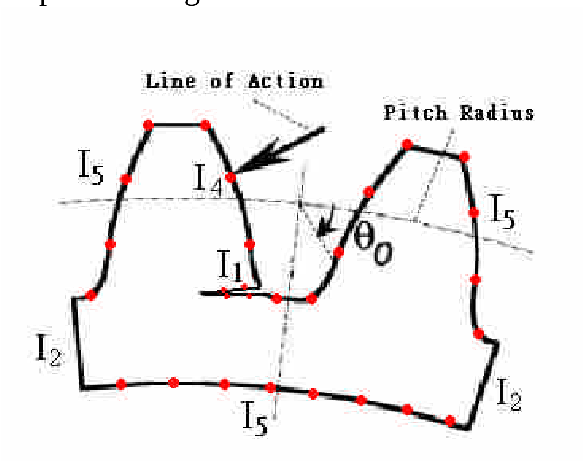

Fig. 19 Schematic of BEM mesh and different regions of cracked ring.

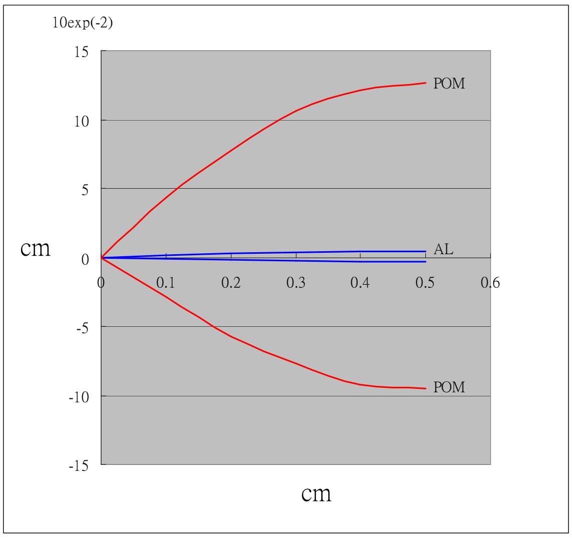

Fig. 20 Comparison between the crack opening displacements of the crack of the gears made of POM and Aluminum Alloy.

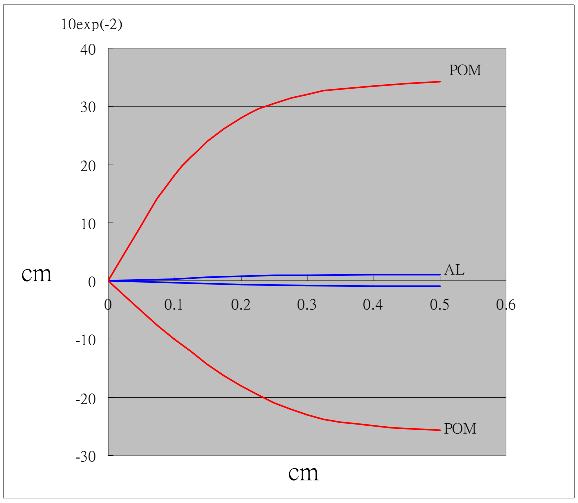

Fig.21 Comparison between the crack shear displacements of the crack of the gears made of POM and Aluminum Alloy.

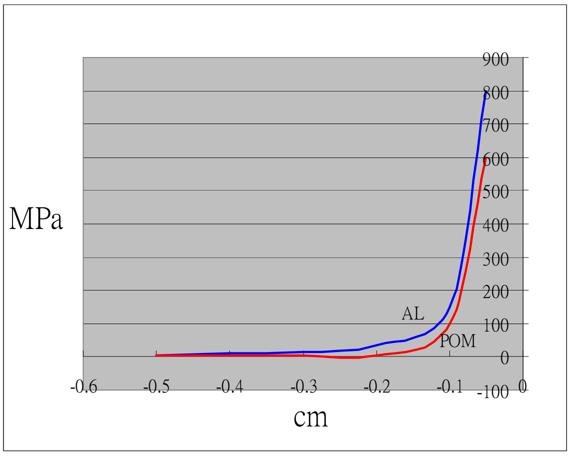

Fig. 22 Comparison between normal stress distributions in the ligament portion of cracked tooth of the gears made of POM and Aluminum Alloy.

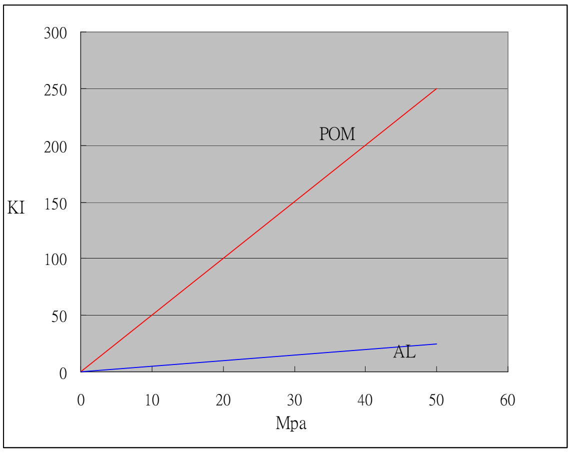

Fig. 24 Comparison between mode I stress intensity factors of the crack the gears made of POM and Aluminum Alloy.

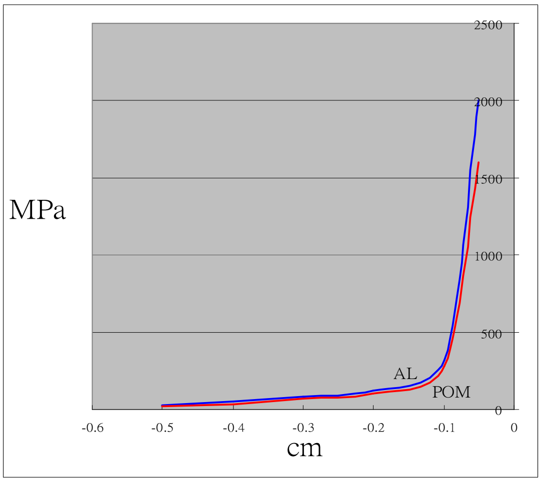

Fig. 23 Comparison between shear stress distributions in the ligament portion of cracked tooth of the gears made of POM and Aluminum Alloy.

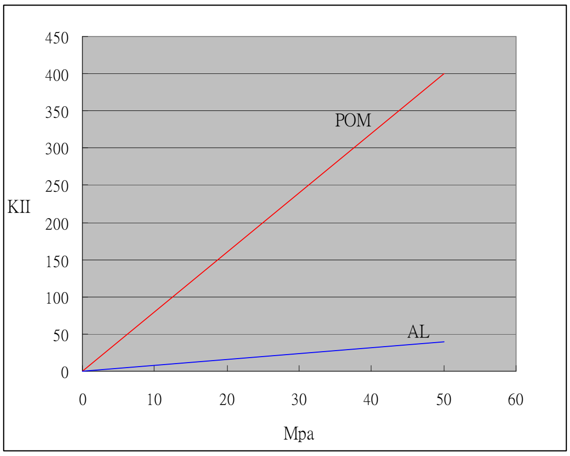

Fig. 25 Comparison between mode II stress intensity factors of the crack the gears made of POM and Aluminum Alloy.

行政院國家科學委員會補助國內專家學者出席國際學術會議報告

99年 4 月 8 日

附件三

報告人姓名	楊立杰	服務機構及職稱	中華大學教授
會議 時間 地點	99年3月27日至99年4月4日 成都四川大學	本會核定補助文號	
會議名稱	(中文)2010兩岸五校數學研討會 (英文)		
發表論文題目	(中文)一些邊界元素在工業上的應用 (英文)Some Boundary Element Applications in Industry		

報告內容應包括下列各項:

一、參加會議經過

3/27日我一大早便由桃園出發,至香港轉成中國國際航空的班機至成都,本來11:10的班機,因為擋風玻璃破裂,必須由北京運送下來,以至於飛機到19:30才由香港起飛,到成都已是晚上22:00,實在有些不敢恭維,還好後面的行程運作順利,總算是不虛此行。

二、與會心得

這次研討會是由兩岸五校(中山、義守、淡江、中華、四川)的十位學者,針對目前的研究領域發表成果,由於時間安排的非常寬鬆,讓我們都能充分的了解每位學者的研究精隨,對自己所從事的研究也有改進的方向,與成長的空間。

三、考察參觀活動(無是項活動者省略)

考察參觀活動是4/3日誌成都市區的參觀,整個市區可能有台北市的三倍大,外環道共分三環,市內也有很多的名勝古蹟,一年前的汶川地震在此也看得到所遺留下的痕跡,整個城市看起來各方面都在建設之中,惜市民不遵守交通規則,衛生習慣不好,讓我對成都的觀感打了折扣。

四、建議

此次活動讓我們增廣見聞,不但了解對岸學者在大學中的學術定為有了更進一步的了解,更對成都居民的生活方式感到好奇,建議以號應多多辦理這方面的學術活動,以增加彼此的了解程度。

五、攜回資料名稱及內容

此次攜回2010年兩岸五校數學研討會演講摘要一份,其中包括二十位學者的近期研究方向與成果,頗具參考價值。

六、其他

行政院國家科學委員會補助國內專家學者出席國際學術會議報告

99 年 6 月 11 日

附件三

報告人姓名	楊立杰	服務機構及職稱	中華大學教授
會議 時間 地點	99 年 6 月 7 日至 99 年 6 月 9 日 馬來西亞，吉隆坡	本會核定補助文號	NSC 98-2218-E-216-001
會議名稱	（中文） （英文）The 8th International Conference on Fracture and Strength of Solids		
發表論文題目	（中文） （英文）NUMERICAL APPLICATION IN WEIGHT REDUCTION OF LATERAL PLATE OF RESCUE ROBOT		

報告內容應包括下列各項：

七、參加會議經過

6/6 日下午 3:05 由桃園出發，搭乘馬來西亞航空公司的班機至吉隆坡，到達住宿的飯店(Istana Hotel)已將近晚上 10 點，原本感覺沒有多遠的行程，前後也花了 7 個多小時。

八、與會心得

這次研討會是由馬來西亞的 Professor M. N. Tamin 主辦，與會者不乏力學界知名學者，針對目前的研究領域發表成果，由於時間安排洽當，讓我們都能充分的利用自己的時間去了解每位學者的研究精隨，對自己所從事的研究也有改進的方向，與成長的空間。

九、考察參觀活動(無是項活動者省略)

馬來西亞的種族是非常複雜的，在最後一天下午的參訪活動中，我充分的了解到這三大民族(馬來、華人、印尼)的融合性與各種不童的發展色彩，吉隆坡是觀光城市，捷運四通八達但稍嫌老舊，整個城市看起來各方面都仍在建設之中，石油雙塔位於吉隆坡市中心，為整個城市增添了不少可看性。

十、建議

此次活動讓我們增廣見聞，不但對別的國家學術發展更有進一步的了解，更對居民的生活方式感到好奇，建議以號應多多參加這方面的學術活動，以增加彼此的了解程度。

十一、 攜回資料名稱及內容

攜回 The 8th International Conference on Fracture and Strength of Solids 演講摘要及 CD 各一份，其中包括與會所有學者近期研究方向與成果，頗具參考價值。

十二、 其他

NUMERICAL APPLICATION IN WEIGHT REDUCTION OF LATERAL PLATE OF RESCUE ROBOT

Lih-jier Young

Department of Applied Mathematics, Chung Hua University

No. 707 Section II, Wu Fu Road, Hsin Chu City

Taiwan 30012, R.O.C.

young@chu.edu.tw

Keywords: Boundary Element Method

Abstract. In general, weight reduction will always lower the strength of the specimen. The primary purpose of this paper is weight reduction of lateral plate of rescue robot without causing the strength of it by using the Boundary Element Method (BEM). The dynamical loading conditions are performed before and after weight reduction. The numerical results of the stress distribution and the plastic deformation along the center line (interface) of the lateral plate show that the endure limits of the plate before and after weight reduction are almost the same and therefore, will not lower the strength of the plate.

Introduction

Earthquakes are so frequently in the world recently which always causing serious damage of the buildings, properties, and injury and death of peoples. Rescue robots with light, thin body are therefore needed in small space of the disaster scene. During weight reduction process the strength of the rescue robot is also evaluated. Several papers show the potential applications of the BEM code to crack problems. Ghorbanpoor and Zhang [1] point out that the accuracy of the BEM prediction is satisfactory when it is compared with results from a finite element solution with very fine mesh and with the analytical solution. Tan and Gao [2] show the powerful application of the BEM in the analysis of biomaterial interface crack problem. Lih-jier Young and Tsai [3] show the powerful application of the BEM in rough contact mixed mode with the plastic crack tip problem and gives the accuracy up to 98.11%. Boundary element method is used to model the complex resistance to the applied field of the lateral plate of rescue robot to find the stress distribution along the interface. The outlook and dimension in mm of the plate are shown in Fig. 1. Young [4] also shows the potential application of the BEM determining the effect of crack face roughness in a realistic experimental specimen. The maximum allowable stress of the plate is defined by both the normal and the shear stress of first point along the interface reach the yield stress σ_y and τ_y, respectively, where $\tau_y = \sigma_y/\sqrt{3}$. The plastic displacement of the interface is obtained by increasing the loading of the plate after the first point yield. Keep increasing the loading and we can get the plastic displacement of the interface.

Dynamical Loading Conditions before Weight Reduction

As discussed in [3], the first step in the BEM solution is to divided the homogeneous medium into two bodies B_γ ($\gamma = 1,2$) along the center line which we call the interface as shown in Fig. 2(a). The interaction between the two bodies included through boundary conditions relating the displacements and stresses on either side of the interface. Let ${}_\gamma t_i$ and ${}_\gamma u_i$ ($\gamma = 1,2$ and $i = 1,2$) denote the ith boundary traction and displacement components, respectively, on the boundary of B_γ. The present model is discretized into 648 nodal points and 4 regions (I_2, I_4, I_5, and I_6) of different types of boundary conditions shown in Fig. 2(a). The interface is denoted by I_2. At points on this region the 2 displacement components and 2 stress components must be continuous. Therefore, the boundary conditions are $({}_2t_1)_{I_2} = -({}_1t_1)_{I_2}$ and $({}_2t_2)_{I_2} = -({}_1t_2)_{I_2}$, $({}_2u_1)_{I_2} = ({}_1u_1)_{I_2}$ and $({}_2u_2)_{I_2} = ({}_1u_2)_{I_2}$. This leaves $({}_1t_1)_{I_2}$, $({}_1t_2)_{I_2}$, $({}_1u_1)_{I_2}$ and $({}_1u_2)_{I_2}$, as the unknowns. Compressive loads are applied through the six pins as in Fig. 3 by assuming a uniform distribution of normal traction over 90 ° of pin hole surfaces (I_6). Therefore, the boundary conditions of these points are $({}_\gamma t_1)_{I_6} = p\cos\theta$ and $({}_\gamma t_2)_{I_6} = p\sin\theta$. The unknowns are $({}_\gamma u_1)_{I_6}$ and $({}_\gamma u_2)_{I_6}$, where p is applied normal stress on the six holes and θ is the angle between the direction normal of each node and x_1-axis as in Fig. 2(a). A concentrate load is also applied through lower half plane point 110 (I_4) The boundary conditions are $({}_1t_2)_{I_4} = p$, $({}_2t_1)_{I_4} = ({}_2t_2)_{I_4} = ({}_1t_1)_{I_4} = 0$ and the unknowns are $({}_\gamma u_1)_{I_4}$ and $({}_\gamma u_2)_{I_4}$. The boundary conditions of the free surfaces (I_5) are $({}_\gamma t_1)_{I_5} = ({}_\gamma t_2)_{I_5} = 0$, and the unknowns are $({}_\gamma u_1)_{I_5}$ and $({}_\gamma u_2)_{I_5}$, where $\gamma = 1$ or 2 depending on whether that portion of I_5 is in B_1 or B_2. Once the points on the interface yield (I_8) in shear direction the boundary conditions are $({}_1t_1)_{I_8} = \sigma_y/\sqrt{3}$, $({}_2t_1)_{I_8} = -\sigma_y/\sqrt{3}$, $({}_1t_2)_{I_8} = -({}_2t_2)_{I_8}$ and $({}_1u_2)_{I_8} = ({}_2u_2)_{I_8}$. The unknowns are $({}_2t_2)_{I_8}$, $({}_1u_1)_{I_8}$, $({}_1u_2)_{I_8}$ and $({}_2u_1)_{I_8}$. For the case both the normal and shear directs yield the boundary conditions are $({}_1t_1)_{I_8} = \sigma_y/\sqrt{3}$, $({}_2t_1)_{I_8} = -\sigma_y/\sqrt{3}$, $({}_1t_2)_{I_8} = \sigma_y$ and $({}_2t_2)_{I_8} = -\sigma_y$.

The BEM consists of the discretization of the boundary surfaces and the numerical approximation of the boundary quantities in the set of equation obtained from the boundary integrals. We model the boundary, using straight-line elements, centered about nodes at which the integrals of the 2D Green's function as in [4]. The final system of simultaneous linear algebraic equations for the unknown nodal displacements and stresses, can be obtained by using Gaussian elimination method.

Figure 4(a) shows the shear stress distribution along the interface. It can be seen that the shear stress of point 100 reaches the yielding criteria in (300 MPa) with the applied load $p = -5.4$ MPa. However, the normal stress is not. We can keep increasing the applied load to $p = -7.1$ Mpa until the normal stress of point 100 reaches the yielding criteria (520 MPa). There are three points, i.e., 100, 99, and 98 yield in shear direction at this moment as shown in Fig. 5(a). Both the shear and normal stresses reach the yielding criteria of points 100, 99, 98, and 97 as in Figs 6(a) and 7(a), respectively, when applied load is up to -7.3 MPa. Figures 8(a) and 9(a) show the plastic displacements both in shear and normal direction of the four yielding point mention above.

Dynamical Loading Conditions after Weight Reduction

The model for the weight reduction lateral plate model is discretized into 904 nodal points and 4 regions (I_2, I_4, I_5, and I_6) of different types of boundary conditions shown in Fig. 2(b). All boundary conditions remain the same as described above. In addition, two rectangular regions with the size $80 \times 46\,\text{mm}^2$ have been cut as shown in Fig. 2(b) which reduce the mass of the plate from 3 kg to 2 kg. The boundary conditions of the inner free surface are the same as the outer one (I_5). The final system of simultaneous linear algebraic equations can also be obtained by using Gaussian elimination method.

Figures 4(b) and 5(b) show the stress distribution along the interface. It can be seen from 4(b) that the shear stress of point 228 reaches the yielding criteria in (300 MPa) with the applied load $p = -4.4$ MPa. However, the normal stress is not. We can keep increasing the applied load to $p = -5.7$ Mpa until the normal stress of point 111 reaches the yielding criteria

(520 MPa). There are three points, i.e., 111, 112, and 228 yield in shear direction at this moment as shown in Fig. 5(b). Both the shear and normal stresses reach the yielding criteria of points 111, 112, and 228, as in Figs 6(b) and 7(b), respectively, when applied load is up to -6.0 MPa. Figures 8(b) and 9(b) show the plastic displacement both in shear and normal direction of the four yielding point mention above.

Conclusions

It can be seen from the results mentioned above that the weight of one lateral plate of the robot have be reduced 1 kg of mass (from 3 kg to 2 kg) but won't lower the strength that much. (allowable stress is reduced from -7.1 MPa to -5.7 MPa). The total mass of one rescue robot may be reduced at least 2 kg after weight reduction and therefore, can moves nimbly during the rescue process.

References

[1] A. Ghobanpoor and J. Zang, "Boundary Elemant Analysis of Crack Growth for Mixed Mode Center Slant Crack Problems," Engineering Fracture Mechanics, Vol. 36, No.5 pp. 661-668, 1990.

[2] C.L. Tan and Y.L. Gao, "Treatment of Bimaterial Interface Crack Problems Using The Boundary Element Method," Engineering Fracture Mechanics, Vol. 36, No. 6, pp. 919-932, 1990.

[3] L.J. Young and Y.P. Tsai, "A Boundary Element Application for Mixed Mode Loading Idealized Sawtooth Fracture Surface," Int'l J. of Solids and Structure, 36, 3239-3252, 1999.

[4] L.J. Young, "An Analysis of a Fracture Specimen for Rough Crack in Shear," Int'l J. of Fracture, 115, 3, 273~285, 2002.

[5] C.A. Brebbia , J.C.F Telles and L.C. Wrobel, " Boundary Element Techniqes ," Springer - Verlag,New York,1970.

Figures

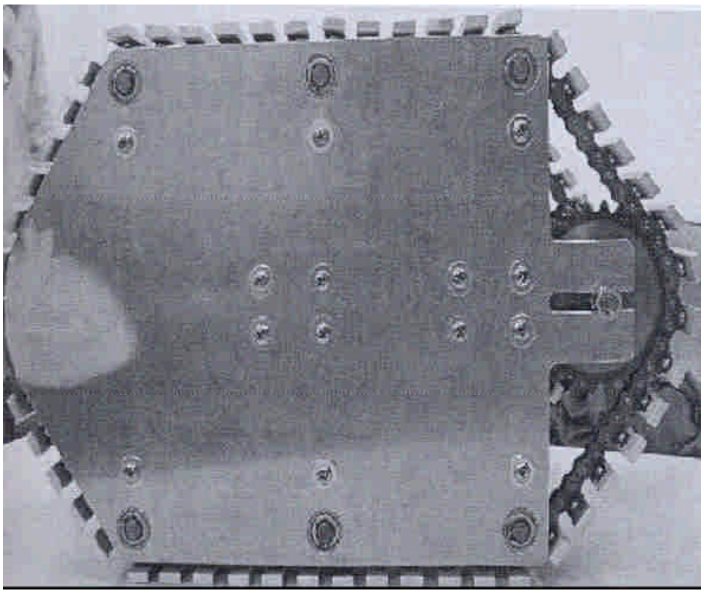

(a)

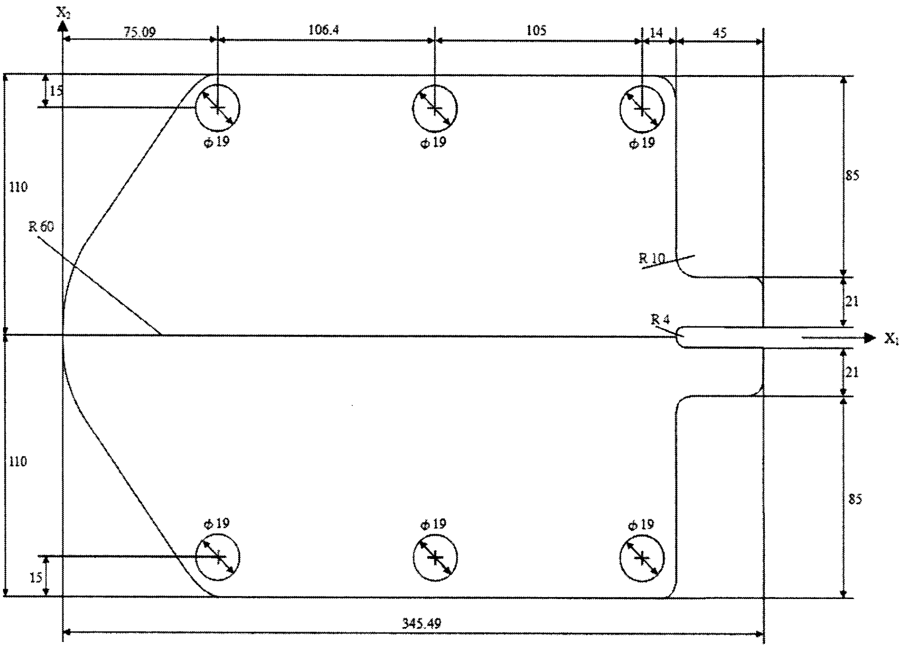

(b)

Fig. 1 (a) Outlook (b) dimension in mm of the lateral plate of rescue robot.

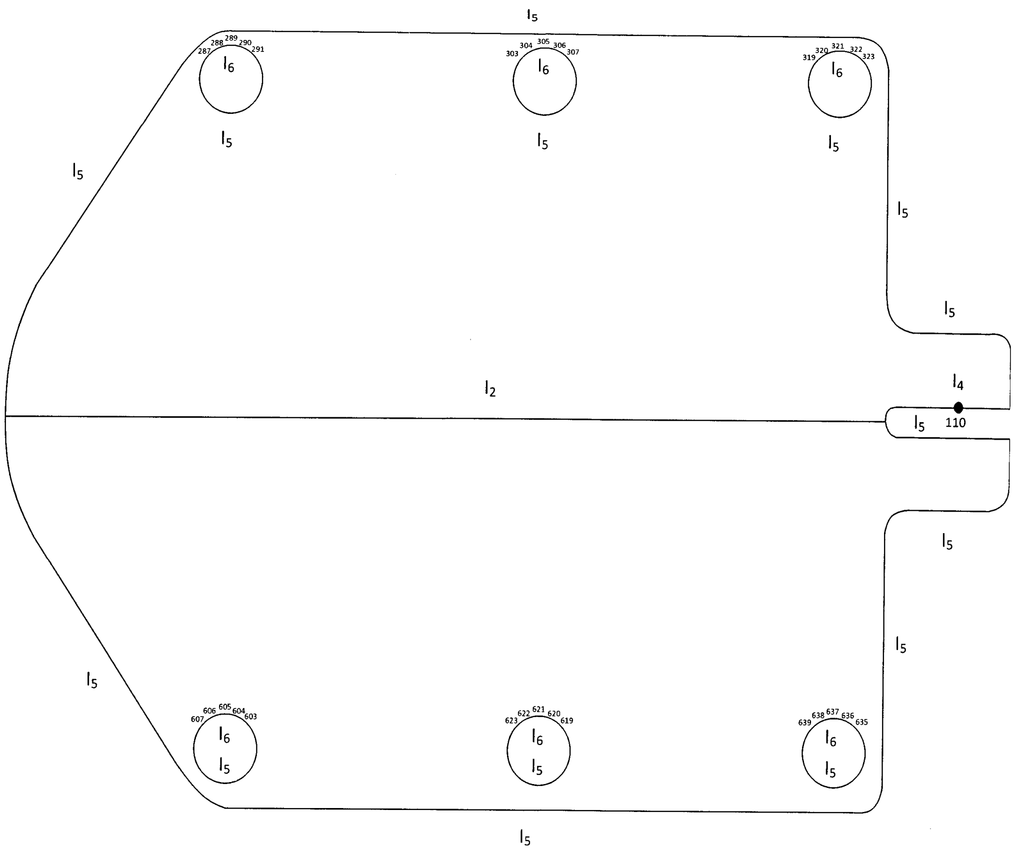

(a)

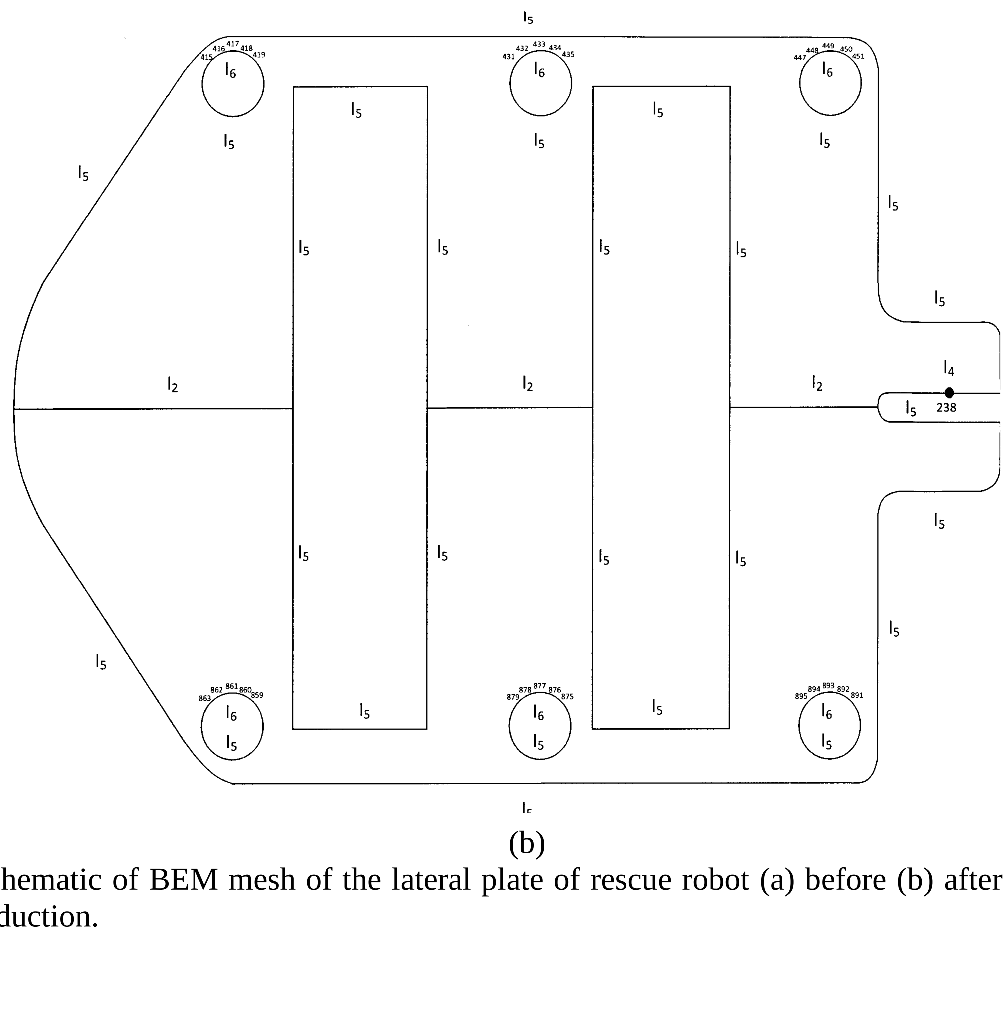

(b)

Fig 2 Schematic of BEM mesh of the lateral plate of rescue robot (a) before (b) after weight reduction.

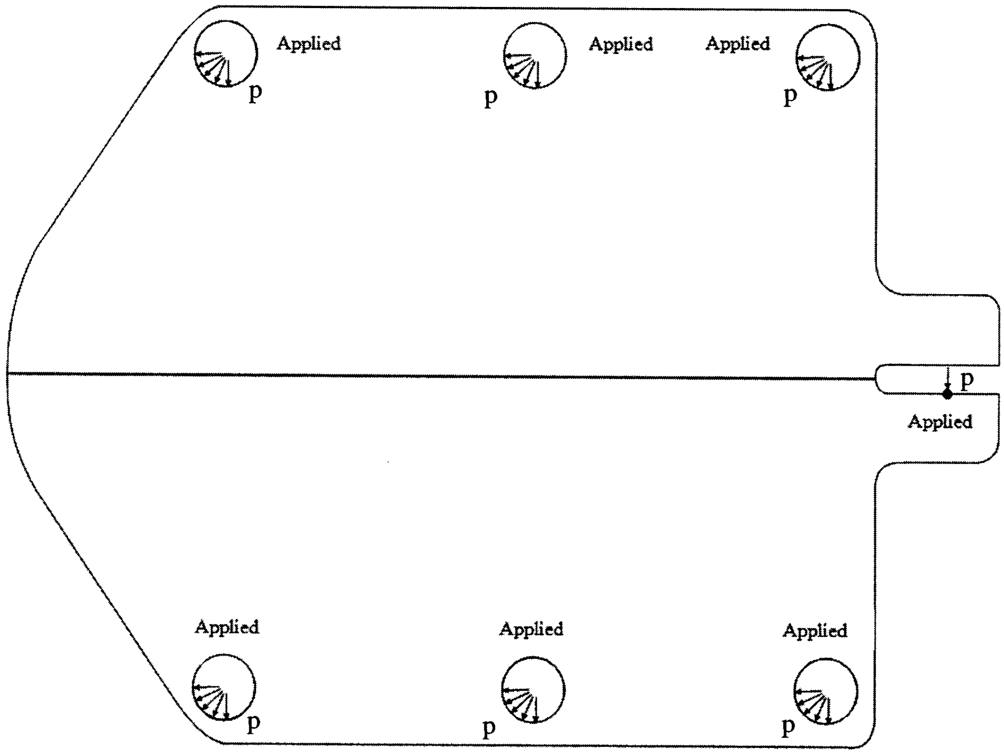

Fig. 3 Loading conditions of the lateral plate of rescue robot.

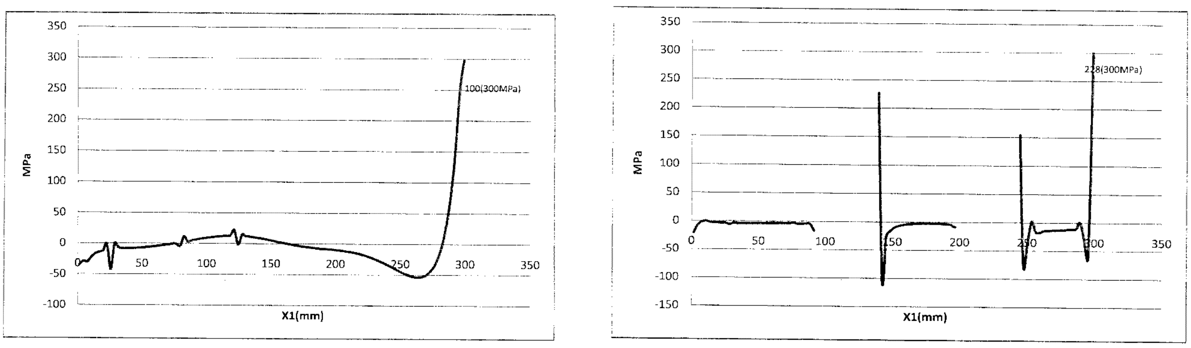

(a) (b)

Fig 4 Shear stress distribution of the interface of the lateral plate (a) before weight reduction with $p = -5.4\,\mathrm{MPa}$ (b) after weight reduction with $p = -4.4\,\mathrm{MPa}$.

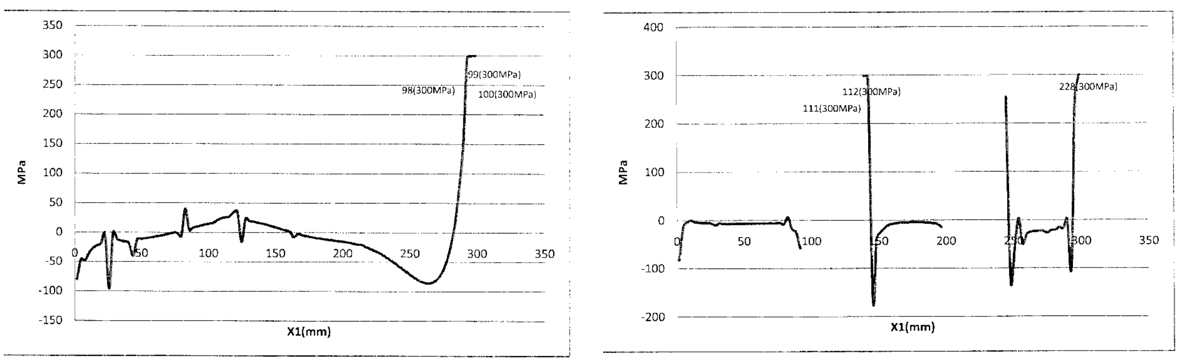

(a) (b)

Fig 5 Shear stress distribution of the interface of the lateral plate (a) before weight reduction with $p = -7.1\,\mathrm{MPa}$ (b) after weight reduction with $p = -5.7\,\mathrm{MPa}$

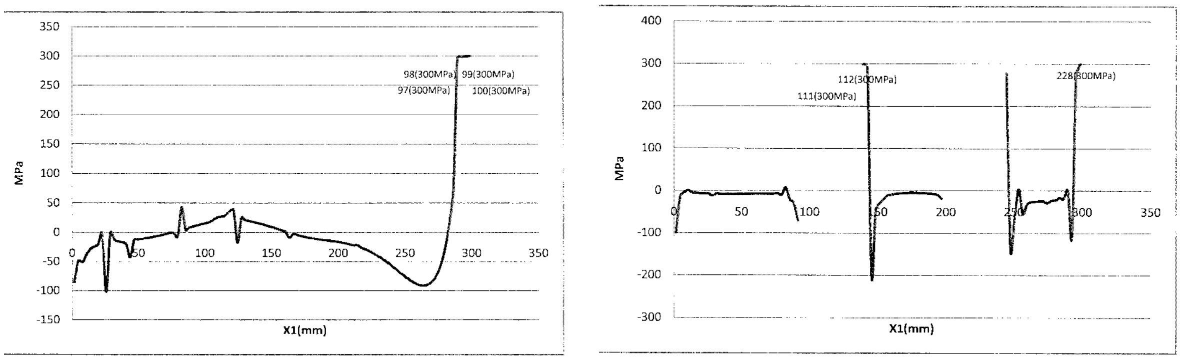

(a) (b)

Fig 6 Shear stress distribution of the interface of the lateral plate (a) before weight reduction with $p = -7.3$ MPa (b) after weight reduction with $p = -6.0$ MPa.

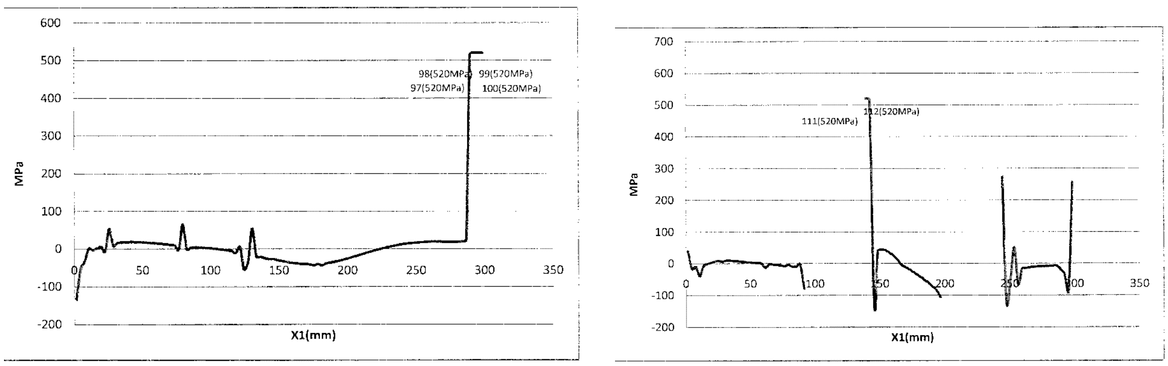

(a) (b)

Fig 7 Normal stress distribution of the interface of the lateral plate (a) before weight reduction with $p = -7.3$ MPa (b) after weight reduction with $p = -6.0$ MPa.

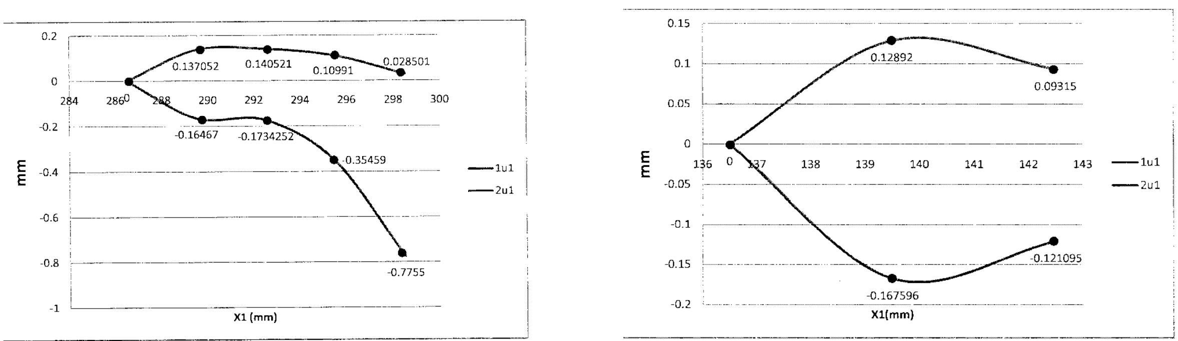

(a) (b)

Figure 8 Plastic deformation in shear direction of the lateral plate (a) before weight reduction with $p = -7.3$ MPa (b) after weight reduction with $p = -6.0$ MPa.

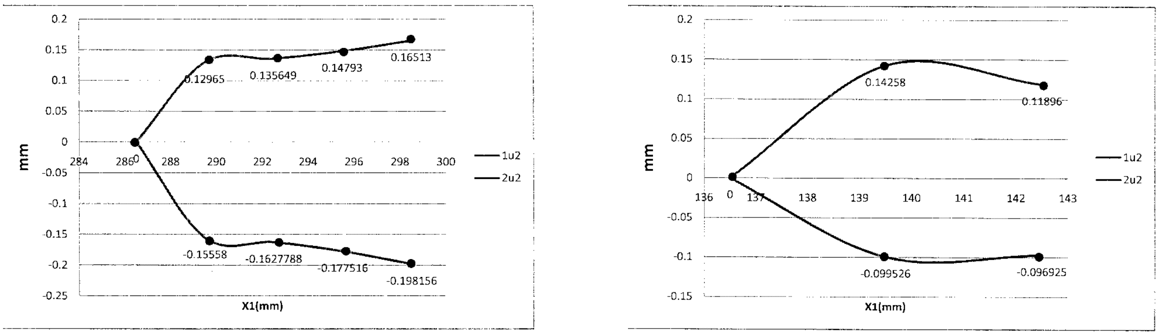

(a) (b)

Figure 9 Plastic deformation in normal direction of the lateral plate (a) before weight reduction with $p = -7.3$ MPa (b) after weight reduction with $p = -6.0$ MPa.

行政院國家科學委員會補助國內專家學者出席國際學術會議報告

99 年 6 月 11 日

附件三

報告人姓名	楊立杰	服務機構及職稱	中華大學教授
會議 時間 地點	99 年 6 月 7 日至 99 年 6 月 9 日 馬來西亞，吉隆坡	本會核定補助文號	NSC 98-2218-E-216-001
會議名稱	（中文） （英文）The 8th International Conference on Fracture and Strength of Solids		
發表論文題目	（中文） （英文）NUMERICAL APPLICATION IN WEIGHT REDUCTION OF LATERAL PLATE OF RESCUE ROBOT		

報告內容應包括下列各項：

一、參加會議經過

6/6 日下午 3:05 由桃園出發，搭乘馬來西亞航空公司的班機至吉隆坡，到達住宿的飯店(Istana Hotel)已將近晚上 10 點，原本感覺沒有多遠的行程，前後也花了 7 個多小時。

二、與會心得

這次研討會是由馬來西亞的 Professor M. N. Tamin 主辦，與會者不乏力學界知名學者，針對目前的研究領域發表成果，由於時間安排洽當，讓我們都能充分的利用自己的時間去了解每位學者的研究精隨，對自己所從事的研究也有改進的方向，與成長的空間。

三、考察參觀活動(無是項活動者省略)

馬來西亞的種族是非常複雜的，在最後一天下午的參訪活動中，我充分的了解到這三大民族(馬來、華人、印尼)的融合性與各種不童的發展色彩，吉隆坡是觀光城市，捷運四通八達但稍嫌老舊，整個城市看起來各方面都仍在建設之中，石油雙塔位於吉隆坡市中心，為整個城市增添了不少可看性。

四、建議

此次活動讓我們增廣見聞，不但對別的國家學術發展更有進一步的了解，更對居民的生活方式感到好奇，建議以號應多多參加這方面的學術活動，以增加彼此的了解程度。

五、攜回資料名稱及內容

攜回 The 8th International Conference on Fracture and Strength of Solids 演講摘要及 CD 各一份，其中包括語彙所有學者近期研究方向與成果，頗具參考價值。

六、其他

無衍生研發成果推廣資料

98 年度專題研究計畫研究成果彙整表

計畫主持人：楊立杰			計畫編號：98-2218-E-216-001-				
計畫名稱：感測網路分散式機器人研發--子計畫一：救援機器人之設計與結構分析(3/3)							
成果項目			量化			單位	備註（質化說明：如數個計畫共同成果、成果列為該期刊之封面故事...等）
			實際已達成數（被接受或已發表）	預期總達成數(含實際已達成數)	本計畫實際貢獻百分比		
國內	論文著作	期刊論文	3	0	100%	篇	
		研究報告/技術報告	0	0	100%		
		研討會論文	7	0	100%		
		專書	0	0	100%		
	專利	申請中件數	0	0	100%	件	
		已獲得件數	0	0	100%		
	技術移轉	件數	0	0	100%	件	
		權利金	0	0	100%	千元	
	參與計畫人力（本國籍）	碩士生	4	0	100%	人次	
		博士生	0	0	100%		
		博士後研究員	0	0	100%		
		專任助理	0	0	100%		
國外	論文著作	期刊論文	4	0	100%	篇	
		研究報告/技術報告	0	0	100%		
		研討會論文	4	0	100%		
		專書	0	0	100%	章/本	
	專利	申請中件數	0	0	100%	件	
		已獲得件數	0	0	100%		
	技術移轉	件數	0	0	100%	件	
		權利金	0	0	100%	千元	
	參與計畫人力（外國籍）	碩士生	0	0	100%	人次	
		博士生	0	0	100%		
		博士後研究員	0	0	100%		
		專任助理	0	0	100%		

其他成果 (無法以量化表達之成果如辦理學術活動、獲得獎項、重要國際合作、研究成果國際影響力及其他協助產業技術發展之具體效益事項等，請以文字敘述填列。)	無

	成果項目	量化	名稱或內容性質簡述
科教處計畫加填項目	測驗工具(含質性與量性)	0	
	課程/模組	0	
	電腦及網路系統或工具	0	
	教材	0	
	舉辦之活動/競賽	0	
	研討會/工作坊	0	
	電子報、網站	0	
	計畫成果推廣之參與（閱聽）人數	0	

國科會補助專題研究計畫成果報告自評表

請就研究內容與原計畫相符程度、達成預期目標情況、研究成果之學術或應用價值（簡要敘述成果所代表之意義、價值、影響或進一步發展之可能性）、是否適合在學術期刊發表或申請專利、主要發現或其他有關價值等，作一綜合評估。

1. 請就研究內容與原計畫相符程度、達成預期目標情況作一綜合評估

■達成目標

□未達成目標（請說明，以 100 字為限）

　　□實驗失敗

　　□因故實驗中斷

　　□其他原因

說明：

2. 研究成果在學術期刊發表或申請專利等情形：

論文：■已發表 □未發表之文稿 □撰寫中 □無

專利：□已獲得 □申請中 ■無

技轉：□已技轉 □洽談中 ■無

其他：（以 100 字為限）

此三年計畫發表了 10 篇期刊論文(4 篇 SCI)，以及 11 篇研討會論文(2 篇國際、2 篇兩岸)

3. 請依學術成就、技術創新、社會影響等方面，評估研究成果之學術或應用價值（簡要敘述成果所代表之意義、價值、影響或進一步發展之可能性）（以 500 字為限）

在救援機器人的設計上便存在著不同大小的圓形環，在第一年計畫中，我們成功的應用邊界元素法，對圓形環承受反向應力情況下產生塑性鉸的位置，塑性鉸的個數將會隨著受力的增加，以及不同的裂縫位置在圓環的不同位置產生，當圓環塑性鉸數目增加至 4 個時，此圓環便會崩塌，此結果不僅與理論敘述一致，精確度達 98%以上，更為救援型機器人所使用的圓環立定了一套有效的邊界元素應力檢測分析模式。

在第二年的計畫中，應用邊界元素法的分析，重量為 3 kgw 的救援機器人的側向板，在經過由挖去兩塊矩形區域的減重處理後，重量便減輕為 2 kgw，而在與未減重的情況相較之下，所能承受的允許強度並不會相差太大，但整個救援型機器人卻因左右兩塊側向板減重的情況下，總共減輕了 2 kgw 的重量。

減重是可以適用在救援型機器人的任何一個工件的，第三年的計畫便是針對齒輪部分，試圖以塑鋼取代鋁合金材料，並應用邊界元素程式分析並加以減重，將救援機器人的重量由原先的 10 公斤重再大幅向下修改至 6 公斤重，大大的增加了本身的靈活與輕巧性。

此三年計畫不但在學術界發表了 10 篇期刊論文，以及 11 篇研討會論文，更讓救援機器人有靈活的身軀，在救災方面能夠發揮更淋漓盡致的效果，在學術，以及應用方面都具有極大的價值。